

Optimal superpositions for particle detection via quantum phase

Eva Kilian¹, Marko Toroš², P. F. Barker¹ and Sougato Bose¹

¹*Department of Physics & Astronomy, University College London, London WC1E 6BT, United Kingdom*

²*School of Physics & Astronomy, University of Glasgow, Glasgow G12 8QQ, United Kingdom*



(Received 12 October 2023; accepted 29 February 2024; published 9 April 2024)

Exploiting quantum mechanics for sensing offers unprecedented possibilities. State-of-the-art proposals for novel quantum sensors often rely on the creation of large superpositions and generally detect a field. However, what is the optimal superposition size for detecting an incident particle from a specific direction? This question is nontrivial as, in general, this incident particle will scatter off with varied momenta, imparting varied recoils to the sensor, resulting in decoherence rather than a well-defined measurable phase. By considering scattering interactions of directional particulate environments with a system in a quantum superposition, we find that there is an optimal superposition size for measuring particles via a relative phase. As a consequence of the anisotropy of the environment, we observe a feature in the limiting behavior of the real and imaginary parts of the system's density matrix, linking the optimality of the superposition size to the wavelength of the scatterer.

DOI: [10.1103/PhysRevResearch.6.023037](https://doi.org/10.1103/PhysRevResearch.6.023037)

I. INTRODUCTION

Quantum sensing with matter-wave interferometers has prompted the development of numerous commercial technologies, offering highly precise sensors. State-of-the-art experiments and proposals encompass research in the areas of metrology [1], gravimetry [2–8], geophysics [9,10], quantum foundational principles [11–16], and sensing for fundamental physics [6,17–24]. While larger quantum objects as a sensor, such as nanoparticles, have typically been prepared in a near-classical or Gaussian initial state [25–27], the full potential of quantum mechanics becomes apparent when non-Gaussian states, such as a state during interferometry, are utilized. Optimization of the experimental setup and parameters in such cases in order to extract exquisitely weak signals is of utmost importance.

The sensing of potentials, such as the gravitational potential near earth, often necessitates the realization of quantum superposition states with large spatial separation δx between the superposed components, since the accumulated phase $\Delta\phi$ increases with increasing separation. For example, an object of mass m held in a quantum superposition of localized states separated vertically by δx for a time interval τ near earth's surface acquires the celebrated Colella-Overhauser-Werner phase of $\Delta\phi \sim mg\delta x\tau/\hbar$ [3,4,28], while the phase due to the curvature of a proximal mass is proportional to $(\delta x)^2$ [7]. For a dynamical monochromatic classical field of wave-number magnitude k , again, while phase $k\delta x$ is defined modulo 2π , it surely does not harm the coherence of the superposition to have $\delta x > 1/k$ [19]. At the other extreme is the detection of particulate matter interacting with the sensing system via a coupling term. This is, however, phenomenologically different

as it cannot be correctly approximated by a classical field. In the latter regime, the focus has been on detection of the particulate source via the decoherence of a quantum superposition, manifested as loss of interference, as the particles scatter off the sensor mass, typically imparting random momenta [20,21,29]. Thus, the measurement of a coherent phase is often not associated with the detection of particles. As far as current understanding goes, the intuition is that if fields are concerned, δx higher is typically better, while for particles, decoherence would be the prime signature.

In this work, we show that neither of the above intuitions is correct for particulate matter incident from a given direction: We find that there exists an optimal superposition size for quantum sensing in scattering experiments, depending on the characteristics of the environmental source. This arises due to a competition between a coherent phase contribution and a decoherence contribution. To illustrate this effect, we consider the blueprint of an incoming particle (the signal) that scatters from a massive quantum system placed in spatial superposition (the sensor) as represented in Fig. 1(a). Working within the framework of open quantum systems, we compute the effects arising from the interaction of the system with a directional particulate environment and discuss to what extent the superposition size impacts the accumulation of the phase. Contrary to expectations, reading the phase imparted due to scattering in the presence of decoherence induced by the same scattering may not be optimized at a trivial point. Aside this fundamental point, we present an application in single-photon and -atom detection. We conclude by discussing the implications of our finding for present-day sensing experiments.

II. SCATTERING MASTER EQUATION

The interaction of a superposed quantum object with gaseous particles and photons can be described using the formalism of open quantum systems. Following the seminal work of Joos and Zeh [30], the mathematical model has been

Published by the American Physical Society under the terms of the [Creative Commons Attribution 4.0 International](https://creativecommons.org/licenses/by/4.0/) license. Further distribution of this work must maintain attribution to the author(s) and the published article's title, journal citation, and DOI.

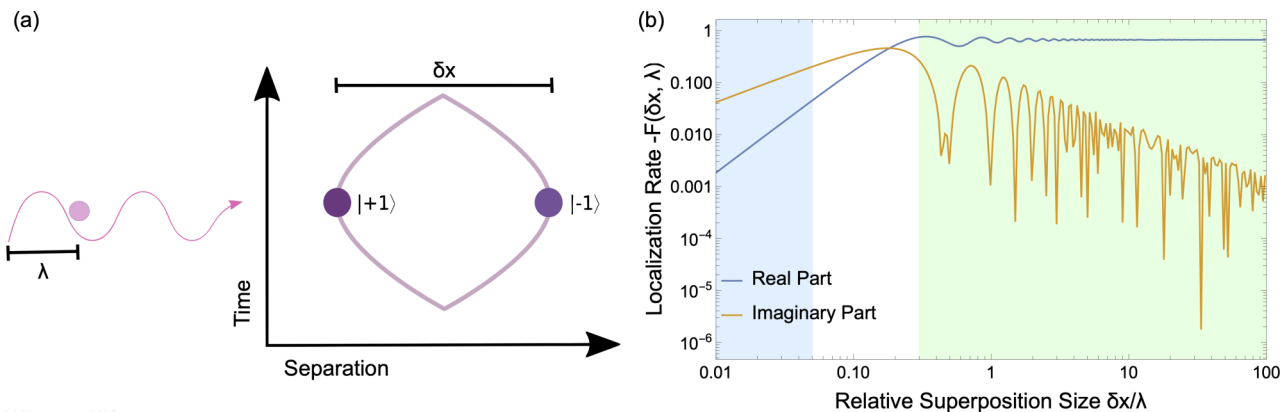


FIG. 1. (a) A particle (pink) scattering from a quantum object (purple spheres) in a Stern-Gerlach-type interferometer, where the sensor's spin-state-dependent evolution is exploited to split and recombine the motional wave packet (purple lines). The incoming particle is sensed through its momentum transfer to the quantum object, which manifests in the appearance of a relative phase between superposed components. (b) Short-wavelength (SW) and long-wavelength (LW) regimes of quantum state evolution for Thompson scattering. Regions shaded indicate the LW regime (blue), the intermediate region (white), and a region that includes the SW regime (green). The quantity λ is the particle's wavelength, δx is the superposition size, and real and imaginary parts indicate the localization rate's contribution to the off-diagonal elements of the system's density matrix. The real part (blue line) is typically used to quantify decoherence. The imaginary part (orange) vanishes in an isotropic situation, where particles are coming randomly from all directions. For a directed source however, the imaginary part can be used to sense particles through relative phases, particularly in regimes where the decoherence contribution is suppressed. The Goldilocks zone for optimal sensing is in the white-shaded region.

extended [31] under the assumption that the scattering of the environment does not significantly disturb the sensor.

Concretely, the reduced density matrix of a system interacting with a particulate environment through scattering [31] is governed by the master equation [32,33]

$$\frac{d\rho_S(\mathbf{x}, \mathbf{x}')}{dt} = \frac{1}{i\hbar} \langle \mathbf{x} | [\hat{H}_S, \hat{\rho}_S] | \mathbf{x}' \rangle - F(\mathbf{x} - \mathbf{x}') \rho_S(\mathbf{x}, \mathbf{x}'), \quad (1)$$

where \hat{H}_S is the Hamiltonian describing the unitary evolution of the sensor, ρ_S is its density matrix, and

$$F(\mathbf{x} - \mathbf{x}') = \int dq n(q) v(q) \int \frac{d\Omega d\Omega'}{4\pi} p(\Omega, \Omega') \times (1 - e^{i(\mathbf{q}-\mathbf{q}')(\mathbf{x}-\mathbf{x}')} |f(\mathbf{q}, \mathbf{q}')|^2). \quad (2)$$

The function $p(\Omega, \Omega')$ is a normalized probability density with incoming (outgoing) scattering angle Ω (Ω'), where $p(\Omega, \Omega') = 1$ is the typical scenario where scatterers impart momentum from all directions. The quantities $n(q)$ and $v(q)$ refer to the number density and speed of particles with wave number q , which is related to their wavelength $\lambda = \frac{2\pi}{q}$ and momentum $\mathbf{p} = \hbar\mathbf{q}$, \mathbf{q} being the wave vector. The scattering amplitude of an interaction process is denoted by $f(\mathbf{q}, \mathbf{q}')$, with \mathbf{q} and \mathbf{q}' labeling incoming and outgoing wave vectors, respectively. Here $F(\mathbf{x} - \mathbf{x}')$ is known as the localization rate. If it is real valued, the sensing system exhibits a loss of coherence over time, while an imaginary contribution manifests in the appearance of a phase $e^{i(\mathbf{q}-\mathbf{q}')(\mathbf{x}-\mathbf{x}')}$. As such, $F(\mathbf{x} - \mathbf{x}')$ should not be simplistically attributed to decoherence as it can contain also a unitary contribution, as we will see. Differences in the phases arising at \mathbf{x} and \mathbf{x}' can be measured and exploited in quantum sensing.

For an incoming particle of wavelength λ , it is useful to investigate two regimes of interest in order to describe the behavior of the sensing system. In the long-wavelength regime,

where $\lambda \gg \delta x$, with $\delta x = |\mathbf{x} - \mathbf{x}'|$, the phase term in Eq. (2) becomes small enough to warrant an approximate treatment of the exponential function by Taylor expanding the argument. Calculating up to second order, a quadratic dependence of the localization rate on the superposition size $F(\mathbf{x} - \mathbf{x}') \propto \frac{1}{2} q^2 (\hat{\mathbf{n}} - \hat{\mathbf{n}}') \cdot (\mathbf{x} - \mathbf{x}')^2$ is revealed. Assuming isotropy of the environment, the linear term averages to zero following integration over terms involving the product of an even and odd function in directions $\hat{\mathbf{n}}$ and $\hat{\mathbf{n}}'$.

Master equations of the form (1) can be mapped to equations of the Lindblad type in position representation and for \hat{L}_k corresponding to the physical observable $\hat{L}_k = \hat{\mathbf{x}}$, the equation that governs the evolution of the system becomes

$$\frac{d\rho_S(\mathbf{x}, \mathbf{x}', t)}{dt} = -\frac{\kappa}{2} (\mathbf{x} - \mathbf{x}')^2 \rho_S(\mathbf{x}, \mathbf{x}', t), \quad (3)$$

assuming the individual sensing system's evolution is negligible. The quantity κ incorporates information contained in the localization rate $F(\mathbf{x} - \mathbf{x}')$ as written in Eq. (2).

In the short-wavelength regime, the exponential function in Eq. (2) oscillates rapidly and hence quickly averages out upon integration. Equation (2), expressed in the form of Eq. (3), tends to

$$\frac{d\rho_S(\mathbf{x}, \mathbf{x}', t)}{dt} = -\frac{\Gamma}{2} (1 - \delta_{\mathbf{x}, \mathbf{x}'}) \rho_S(\mathbf{x}, \mathbf{x}', t), \quad (4)$$

where, for a qualitative understanding, we have taken a discrete set of \mathbf{x} values and $\delta_{\mathbf{x}, \mathbf{x}'}$ is a Kronecker delta. Information contained in $F(\mathbf{x} - \mathbf{x}')$ is incorporated in Γ . If a given environment is not isotropic and the scattering particles are instead impinging from a specific direction, the limiting behaviors reveal the emergence of an optimal superposition size where the detection of the particle is also from the phase imparted. To demonstrate this effect, we resort to a combination of analytic

TABLE I. Limiting behavior of the sensing system's off-diagonal density-matrix elements. The real-part behavior follows the theoretically predicted trends as observed in random uniform scattering. For a nonuniform environment, the imaginary part [$O(2)$] behaves drastically differently and is nonvanishing.

Limit	Real part	Imaginary part
Long wavelength	$\propto \delta x^2$	$\propto \delta x$
Short wavelength	$\Gamma = \text{const}$	$\rightarrow 0$

approximations and exact numerics of the reduced system density matrix for explicit examples.

III. EMERGENCE OF AN OPTIMAL SUPERPOSITION SIZE FOR PARTICLE DETECTION

To illustrate the emergence of an optimal superposition size we focus on two cases [31], with differential cross sections

$$|f(\mathbf{q}, \mathbf{q}')|^2 = gq^j \frac{1}{2} \left(1 + \left| \frac{\mathbf{q}\mathbf{q}'}{q^2} \right|^2 \right). \quad (5)$$

For the expansion order $j = 0$ and $g = r_e^2$ with r_e the square of the classical electron radius, we recover a differential cross section for Thompson scattering, while values of $j = 4$ and $g = a^6 \left| \frac{\epsilon - 1}{\epsilon + 1} \right|^2$ with a as the scatterer's radius and ϵ the dielectric constant describe Rayleigh scattering.

Let us assume the particles travel along the z axis and the superposition is oriented along z . In the long-wavelength limit, we expand the exponent in Eq. (2) in orders of δx and choose $p(\Omega, \Omega') = \delta(\theta)\delta(\phi)/\sin\theta$ for a spherical coordinate system. Further, we select the coordinates of our wave vectors to be $\mathbf{q} = q(0, 0, 1)$ and $\mathbf{q}' = q(\cos\varphi' \sin\theta', \sin\varphi' \sin\theta', \cos\theta')$, notably keeping the magnitude unchanged, which is a valid approximation for negligible momentum transfers. If $j = 0$, Taylor expansion to second order in δx and subsequent angular integration result in

$$F(\mathbf{x} - \mathbf{x}') = \int dq n(q) v(q) g \left[-\frac{2}{3} i q \delta x + \frac{7}{15} q^2 \delta x^2 + O(\delta x^3) \right]. \quad (6)$$

Similarly, we obtain a barely modified equation for $j = 4$. For both cases, we observe the emergence of an imaginary linear (Hamiltonian) term in the master equation [34,35] (see Table I), showing the possibility of detecting particles by a phase. Importantly, this behavior appears to be independent of the exact form of the differential scattering cross section, surfacing merely due to directional momentum impartment.

The limit of small wavelengths is difficult to treat analytically due to the oscillatory behavior of the integrand. The complexity of the problem can however be reduced by assuming the geometry described in this section. Using the Jacobi-Anger expansion, the trigonometric function in our exponential is expressed in the basis of its cylindrical harmonics via the relation $e^{iz \cos\theta} = J_0 + 2 \sum_{n=1}^{\infty} i^n J_n(z) \cos n\theta$. This enables numerical evaluation of the real and imaginary parts of $F(\mathbf{x} - \mathbf{x}')$ and the signals in various phase measurements.

In what follows we assume a very narrow distribution of incoming momenta and hence wave-number magnitude $\delta(q - q_0)$. Figure 1(b) displays the trend of the real and imaginary parts for multiple values of $\frac{\delta x}{\lambda}$, where the factor $g = r_e^2$ has been neglected. In the small- $\frac{\delta x}{\lambda}$ limit, the full numerics match with the polynomially increasing behavior of the imaginary (linear) and real (quadratic) parts as given by Eq. (6). Moreover, the visible decay of the imaginary phase contribution to zero and the saturation of the real part confirm the expected limiting behavior for large values of $\frac{\delta x}{\lambda}$ in the short-wavelength limit. However, *how* these limits are reached differs drastically from the case of random uniform scattering, where the exponential contribution habitually averages out (standard setting of decoherence due to scatterers [30,31]).

The second example for $j = 4$ reveals a similar trend, though the localization function is scaled by a factor q^4 and the coupling g is changed. Employing previous calculational methods will nonetheless lead to the same qualitative observation, the emergence of an optimal ‘‘Goldilocks zone’’ for the accumulation of phase as depicted in Fig. 1, where the zone is shaded in white and the phase imparted is optimal for $\delta x \sim 0.2\lambda$.

IV. EXPERIMENTAL SIGNATURE

The field of matter-wave interferometry offers a catalog of schemes enabling the extraction of the phase contribution due to scattering. A popular approach is founded in the Stern-Gerlach interferometry of spin-mechanical systems [11,36] [see Fig. 1(a)], where the magnetic manipulation of a test mass with an embedded spin is used. After initialization of the sensing system in a center-of-mass motional state $|c\rangle$ and a superposition of spin states $\frac{1}{\sqrt{2}}(|+1\rangle + |-1\rangle)$, the system is allowed to evolve. This evolution leads to a spatial splitting of the center of mass, resulting in the quantum state $|\psi(t)\rangle = \frac{1}{\sqrt{2}}[|c_{s=+1}(t)\rangle|+1\rangle + |c_{s=-1}(t)\rangle|-1\rangle]$. The difference ϕ in distinct phases arising between superposed components can be measured upon completion of the interferometer purely from the spin states. In the ideal case of no decoherence, it becomes $\frac{1}{\sqrt{2}}(|+1\rangle + e^{i\phi}|-1\rangle)$. In presence of a decoherence term $A \sim e^{-\Gamma t}$, the density matrix of the spin at the end of the interferometry becomes

$$\rho = \frac{1}{2} \begin{pmatrix} a & A e^{i\phi} \\ A e^{-i\phi} & b \end{pmatrix}. \quad (7)$$

As the elements of the density matrix will be estimated from probabilities of various measurements, the exponentially decaying decoherence term A is less good as an estimator than $A e^{\pm i\phi}$ when $A \sim 1$. Thus, the phase effect found here from a directional source of particles presents an important method to detect them in comparison to the decoherence they produce. A method of extracting phase differences between the off-diagonal components is to apply $\pi/2$ -phase (S) and Hadamard (H) gate transformations to the quantum state, resulting in a projection of the phases onto the diagonal elements of the density matrix $\rho_f = HS\rho S^\dagger H$,

$$\rho_f = \frac{1}{4} \begin{pmatrix} a + b + 2A \sin\phi & a - b + 2iA \cos\phi \\ a - b - 2iA \cos\phi & a + b - 2A \sin\phi \end{pmatrix}. \quad (8)$$

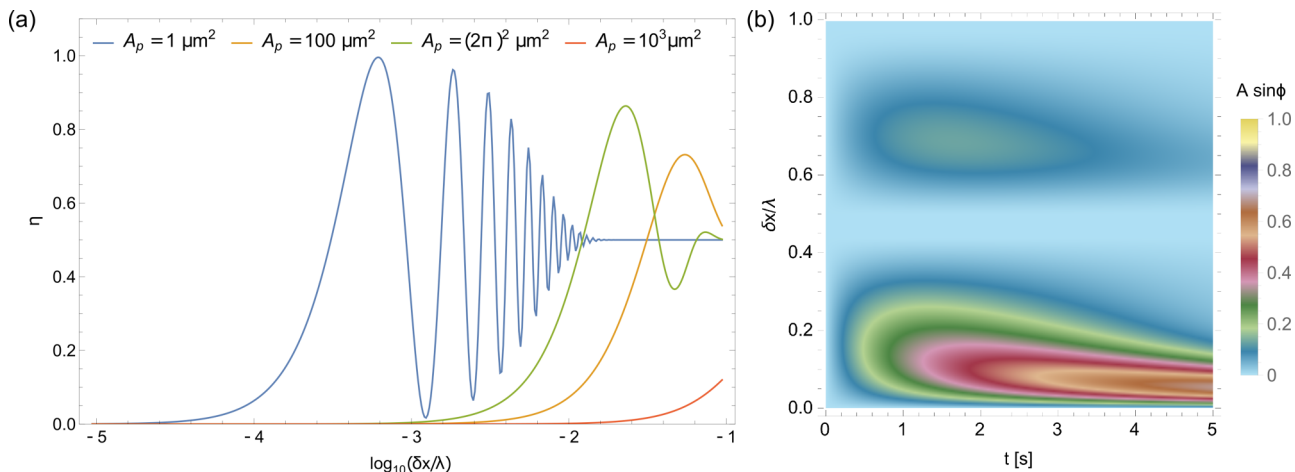


FIG. 2. (a) Quantum efficiency η for Rayleigh scattering of single photons with $\lambda = 1064$ nm on a $0.1\text{-}\mu\text{m}$ -diam sphere for different spatial photon profiles A_p , assuming an estimated flux of 10^6 photons per area A_p per second. (b) Measurable signal (depth coloration) for varying ratios of $\frac{\delta x}{\lambda}$ over a time interval $t = [0, 5]$ s, illustrated for Thompson-type scattering with the exponentiation index $j = 0$ in Eq. (5) when taking the momentum distribution to be a δ function (i.e., around $q = q_0 = 2\pi/\lambda$) and setting the incident particle flux to be such that $\int g n(q)v(q)dq \approx 1$. The orange colored region indicates the maximization of the phase signature in the long-wavelength limit for the lower island, which is also indicated by the nonvanishing first-order contribution in Eq. (6). Depending on the narrowness of the momentum distribution, the behavior of the signal should exhibit similar features for atom scattering.

Subtracting the probabilities $\rho_{f,11} - \rho_{f,22} = A \sin \phi$ relates to the sine of the accumulated phase. This experimental signature is plotted in Fig. 2(b) for the normalized initial state where $\rho_{11} = \rho_{22} = \rho_{12} = \rho_{21} = \frac{1}{2}$ and evolved final states with varying values $\phi = 2\pi\delta x/\lambda$, at times $t = [0, 5]$ s. Concentrating on qualitative aspects of the core issue, i.e., the results of angular averaging over outgoing momenta, we have not chosen a specific distribution for the number density and speed of the particles and taken the momentum distribution to be a δ function (definite wave number around $q = q_0$) and set the incident flux of the particles to be such that $\int g n(q)v(q)dq \approx 1$, effectively plotting the contributions from $F(x - x')$ resulting from the angular integrations. Specific values for these quantities and subsequent integration over the wave numbers will lead to a shifted optimal range for the relative superposition size $\frac{\delta x}{\lambda}$. Although we do not strictly define optimality, relative superposition sizes leading to a phase contribution of $O(1)$ are considered as such. Benchmarking the range of suitable values for $\frac{\delta x}{\lambda}$ to, say, $\sin \phi = 0.95$ is one possible way of defining the window of optimality. For larger or smaller fluxes, the time needed for $O(1)$ will be appropriately scaled.

A. Single-photon detection

As an example of experimental applicability, we analyze the potential benefit of this effect for the detection of spatially shaped single photons, such as those emitted from a quantum-dot source [37,38]. Aiming to operate our sensor as a click detector, we introduce the detection efficiency

$$\eta = \langle -|\rho_{\text{in}}(\tau)|-\rangle = \frac{1}{2}\{1 - [\rho_{12}(\tau) + \rho_{21}(\tau)]\}. \quad (9)$$

The efficiency η , where $\tau = 1$ s, quantifies the distinguishability of a system initially prepared in a superposition state $\rho_{\text{in}} = |+\rangle\langle+|$ from its final state. If the scattering of a photon produces a π phase shift, η approaches its maximum.

Figure 2(a) shows the crucial dependence of η on the ratio $\frac{\delta x}{\lambda}$ for different magnitudes of spatial photon profiles A_p . The single-photon transverse area corresponds to the inverse of $n(q)v(q)\tau$ and $n(q)v(q)\tau \sim 10^6/A_p$. Whereas certain choices of the superposition size will be suitable for operating our sensor as a single-photon detector, others will result in phase shifts that render the system insensitive to the signal, implying that the superposition size can be used for wavelength selection. As seen in Fig. 2(a), sensing will be possible within the peaked regions of relatively broad bands.

B. Detection of single atomic ions

Rutherford scattering of an atomic ion on a nanoparticle of radius $1 \mu\text{m}$ is described via the differential cross section

$$|f(\mathbf{q}, \mathbf{q}')|^2 = \frac{m^2}{\hbar^4 q^4} \frac{(ZZ'e^2)^2}{(4\pi\epsilon_0)^2} \left(1 + \left|\frac{\mathbf{q}\mathbf{q}'}{q^2}\right|^2\right), \quad (10)$$

where Ze and $Z'e$ are the charges of the atom and nanoparticle, $m = 10^{-25}$ kg is the mass of a heavy atom, and ϵ_0 is the vacuum permittivity. We assume an atomic momentum determined via $k_B T/2 = \hbar^2 \mathbf{q}^2/2m$, at a temperature $T = 100$ K. Inserting into Eq. (10) yields

$$|f(\mathbf{q}, \mathbf{q}')|^2 = 10^{-14} Z'^2 \left(1 + \left|\frac{\mathbf{q}\mathbf{q}'}{q^2}\right|^2\right), \quad (11)$$

where the atom's charge number $Z = 1$ is assumed. We hence propose that a $1\text{-}\mu\text{m}$ -diam nanoparticle is able to detect about one atomic ion per second if the atom has a wave-function cross section of 10^4 nm^2 for small values of Z' and the atomic flux is approximately $10^{-4} \text{ s}^{-1} \text{ nm}^{-2}$.

V. SUMMARY

Our observations are of critical relevance to experiments where a particle stream scattering from a superposition has

a unique direction and the environment cannot be treated in the fashion of an isotropic bath. Conversely, we expect that a similar observation can be made for a superposed object that propagates with a given velocity with respect to the environment, such as a crystal with horizontal velocity in a motional superposition state moving through a gas of particles in the laboratory frame.

Considering two limiting regimes for the wavelength of a scatterer interacting with a quantum sensor, we numerically showed that the imaginary contribution arising due to the interaction is, in specific scenarios, nonvanishing and provided a strong argument that the behavior is likely universal. The described relative phase may be used for the detection of weak environmental signatures.

Moreover, we observed the emergence of an optimal parameter choice for the superposition size δx when it comes to measuring special particulate environments and identified a Goldilocks zone. We also showed that the superposition sensor is capable of detecting single photons and single charged atoms with appropriate settings.

Our findings will doubtlessly result in improvements of state-of-the-art quantum sensors and may be utilized to enhance signals which are typically difficult to capture. Several emergent experiments [3,6,21,39] rely on the acceleration of the quantum sensor. Any such setup will be influenced by nonisotropic sources. We therefore emphasize the importance of the choice of the superposition size in relation to phase contributions arising through directional effects.

ACKNOWLEDGMENTS

E.K. would like to acknowledge support from the Engineering and Physical Sciences Research Council (Grant No. EP/L015242/1) and an EPSRC Doctoral Prize Fellowship (Grant No. EP/W524335/1). M.T. would like to acknowledge funding by the Leverhulme Trust (Grant No. RPG-2020-197). S.B. would like to acknowledge EPSRC (Grants No. EP/N031105/1 and No. EP/S000267/1) and Grant No. ST/W006227/1. P.F.B. acknowledges funding from the EPSRC Grant No. EP/W029626/1.

-
- [1] L. Pezzè, A. Smerzi, M. K. Oberthaler, R. Schmied, and P. Treutlein, Quantum metrology with nonclassical states of atomic ensembles, *Rev. Mod. Phys.* **90**, 035005 (2018).
- [2] P. Asenbaum, C. Overstreet, T. Kovachy, D. D. Brown, J. M. Hogan, and M. A. Kasevich, Phase shift in an atom interferometer due to spacetime curvature across its wave function, *Phys. Rev. Lett.* **118**, 183602 (2017).
- [3] M. Scala, M. S. Kim, G. W. Morley, P. F. Barker, and S. Bose, Matter-wave interferometry of a levitated thermal nanoscillator induced and probed by a spin, *Phys. Rev. Lett.* **111**, 180403 (2013).
- [4] C. Wan, M. Scala, G. W. Morley, A. A. Rahman, H. Ulbricht, J. Bateman, P. F. Barker, S. Bose, and M. S. Kim, Free nano-object Ramsey interferometry for large quantum superpositions, *Phys. Rev. Lett.* **117**, 143003 (2016).
- [5] S. Qvarfort, A. Serafini, P. F. Barker, and S. Bose, Gravimetry through non-linear optomechanics, *Nat. Commun.* **9**, 3690 (2018).
- [6] R. J. Marshman, A. Mazumdar, G. W. Morley, P. F. Barker, S. Hoekstra, and S. Bose, Mesoscopic interference for metric and curvature & gravitational wave detection, *New J. Phys.* **22**, 083012 (2020).
- [7] M. Toroš, T. W. van de Kamp, R. J. Marshman, M. S. Kim, A. Mazumdar, and S. Bose, Relative acceleration noise mitigation for nanocrystal matter-wave interferometry: Applications to entangling masses via quantum gravity, *Phys. Rev. Res.* **3**, 023178 (2021).
- [8] M.-Z. Wu, M. Toroš, S. Bose, and A. Mazumdar, Quantum gravitational sensor for space debris, *Phys. Rev. D* **107**, 104053 (2023).
- [9] Y. Bidel, N. Zahzam, C. Blanchard, A. Bonnin, M. Cadoret, A. Bresson, D. Rouxel, and M. F. Lequentrec-Lalancette, Absolute marine gravimetry with matter-wave interferometry, *Nat. Commun.* **9**, 627 (2018).
- [10] B. Stray, A. Lamb, A. Kaushik, J. Vovrosh, A. Rodgers, J. Winch, F. Hayati, D. Boddice, A. Stabrawa, A. Niggebaum, M. Langlois, Y.-H. Lien, S. Lellouch, S. Roshanmanesh, K. Ridley, G. de Villiers, G. Brown, T. Cross, G. Tuckwell, A. Faramarzi *et al.*, Quantum sensing for gravity cartography, *Nature (London)* **602**, 590 (2022).
- [11] S. Bose, A. Mazumdar, G. W. Morley, H. Ulbricht, M. Toroš, M. Paternostro, A. A. Geraci, P. F. Barker, M. S. Kim, and G. Milburn, Spin entanglement witness for quantum gravity, *Phys. Rev. Lett.* **119**, 240401 (2017).
- [12] C. Marletto and V. Vedral, Gravitationally induced entanglement between two massive particles is sufficient evidence of quantum effects in gravity, *Phys. Rev. Lett.* **119**, 240402 (2017).
- [13] S. Bose, A. Mazumdar, M. Schut, and M. Toroš, Entanglement witness for the weak equivalence principle, *Entropy* **25**, 448 (2023).
- [14] D. Biswas, S. Bose, A. Mazumdar, and M. Toroš, Gravitational optomechanics: Photon-matter entanglement via graviton exchange, *Phys. Rev. D* **108**, 064023 (2023).
- [15] Y. Margalit, O. Dobkowski, Z. Zhou, O. Amit, Y. Japha, S. Moukouri, D. Rohrlich, A. Mazumdar, S. Bose, C. Henkel, and R. Folman, Realization of a complete Stern-Gerlach interferometer: Toward a test of quantum gravity, *Sci. Adv.* **7**, eabg2879 (2021).
- [16] B. Yi, U. Sinha, D. Home, A. Mazumdar, and S. Bose, Massive spatial qubits: Testing macroscopic nonclassicality and Casimir entanglement, *Phys. Rev. Res.* **5**, 033202 (2023).
- [17] S. Dimopoulos, P. W. Graham, J. M. Hogan, M. A. Kasevich, and S. Rajendran, Gravitational wave detection with atom interferometry, *Phys. Lett. B* **678**, 37 (2009).
- [18] W. Chaibi, R. Geiger, B. Canuel, A. Bertoldi, A. Landragin, and P. Bouyer, Low frequency gravitational wave detection with ground-based atom interferometer arrays, *Phys. Rev. D* **93**, 021101(R) (2016).
- [19] A. A. Geraci and A. Derevianko, Sensitivity of atom interferometry to ultralight scalar field dark matter, *Phys. Rev. Lett.* **117**, 261301 (2016).

- [20] C. J. Riedel, Direct detection of classically undetectable dark matter through quantum decoherence, *Phys. Rev. D* **88**, 116005 (2013).
- [21] J. Bateman, I. McHardy, A. Merle, T. R. Morris, and H. Ulbricht, On the existence of low-mass dark matter and its direct detection, *Sci. Rep.* **5**, 8058 (2015).
- [22] C. J. Riedel and I. Yavin, Decoherence as a way to measure extremely soft collisions with dark matter, *Phys. Rev. D* **96**, 023007 (2017).
- [23] Y. Du, C. Murgui, K. Pardo, Y. Wang, and K. M. Zurek, Atom interferometer tests of dark matter, *Phys. Rev. D* **106**, 095041 (2022).
- [24] E. Kilian, M. Toroš, F. F. Deppisch, R. Saakyan, and S. Bose, Requirements on quantum superpositions of macro-objects for sensing neutrinos, *Phys. Rev. Res.* **5**, 023012 (2023).
- [25] G. Afek, D. Carney, and D. C. Moore, Coherent scattering of low mass dark matter from optically trapped sensors, *Phys. Rev. Lett.* **128**, 101301 (2022).
- [26] S. C. Burd, R. Srinivas, J. J. Bollinger, A. C. Wilson, D. J. Wineland, D. Leibfried, D. H. Slichter, and D. T. C. Allcock, Quantum amplification of mechanical oscillator motion, *Science* **364**, 1163 (2019).
- [27] D. Carney, G. Krnjaic, D. C. Moore, C. A. Regal, G. Afek, S. Bhave, B. Brubaker, T. Corbitt, J. Cripe, N. Crisosto *et al.*, Mechanical quantum sensing in the search for dark matter, *Quantum Sci. Technol.* **6**, 024002 (2021).
- [28] R. Colella, A. W. Overhauser, and S. A. Werner, Observation of gravitationally induced quantum interference, *Phys. Rev. Lett.* **34**, 1472 (1975).
- [29] P. Fragolino, M. Schut, M. Toroš, S. Bose, and A. Mazumdar, Decoherence of a matter-wave interferometer due to dipole-dipole interactions, *Phys. Rev. A* **109**, 033301 (2024).
- [30] E. Joos and H. D. Zeh, The emergence of classical properties through interaction with the environment, *Z. Phys. B* **59**, 223 (1985).
- [31] M. R. Gallis and G. N. Fleming, Environmental and spontaneous localization, *Phys. Rev. A* **42**, 38 (1990).
- [32] K. Hornberger and J. E. Sipe, Collisional decoherence reexamined, *Phys. Rev. A* **68**, 012105 (2003).
- [33] K. Hornberger, S. Utenthaler, B. Brezger, L. Hackermüller, M. Arndt, and A. Zeilinger, Collisional decoherence observed in matter wave interferometry, *Phys. Rev. Lett.* **90**, 160401 (2003).
- [34] J. Schmiedmayer, M. S. Chapman, C. R. Ekstrom, T. D. Hammond, S. Wehinger, and D. E. Pritchard, Index of refraction of various gases for sodium matter waves, *Phys. Rev. Lett.* **74**, 1043 (1995).
- [35] B. Vacchini and K. Hornberger, Quantum linear Boltzmann equation, *Phys. Rep.* **478**, 71 (2009).
- [36] R. J. Marshman, A. Mazumdar, R. Folman, and S. Bose, Constructing nano-object quantum superpositions with a Stern-Gerlach interferometer, *Phys. Rev. Res.* **4**, 023087 (2022).
- [37] M. T. Rakher, L. Ma, M. Davanço, O. Slattery, X. Tang, and K. Srinivasan, Simultaneous wavelength translation and amplitude modulation of single photons from a quantum dot, *Phys. Rev. Lett.* **107**, 083602 (2011).
- [38] L. Hanschke, K. A. Fischer, S. Appel, D. Lukin, J. Wierzbowski, S. Sun, R. Trivedi, J. Vučković, J. J. Finley, and K. Müller, Quantum dot single-photon sources with ultra-low multi-photon probability, *npj Quantum Inf.* **4**, 43 (2018).
- [39] M. Rademacher, J. Millen, and Y. L. Li, Quantum sensing with nanoparticles for gravimetry: When bigger is better, *Adv. Opt. Technol.* **9**, 227 (2020).